RSC Advances

ROYAL SOCIETY OF CHEMISTRY

www.rsc.org/advances

RSC Advances

ARTICLE

Electrochemical reduction of hydrogen peroxide by nanostructured hematite modified electrodes

Received 00th January 20xx,
Accepted 00th January 20xx

DOI: 10.1039/x0xx00000x

www.rsc.org/

Chia-Ting Chang and Chia-Yu Lin*

In this study, various nanostructured hematite (α-Fe_2O_3), including nanorods (α-Fe_2O_{3NR}), nanoparticles (α-Fe_2O_{3Np}), and nanosheets (α-Fe_2O_{3NS}), were synthesized and their electrocatalytic properties towards the reduction of H_2O_2 were investigated. All nanostructured α-Fe_2O_3 were synthesized by using chemical bath deposition (CBD) at mild conditions, followed by thermal treatment at 500 ^{o}C. The nanostructure was controlled simply by adjusting the composition of precursor solution and reaction duration for CBD process. It was found that iron phosphate ($FePO_4$) was deposited *in-situ* onto the surface of these nanostructured α-Fe_2O_3 during the electrochemical pretreatment in the phosphate electrolyte, and both $FePO_4$ and α-Fe_2O_3 showed the activity in catalysing the electrochemical reduction of H_2O_2. In addition, the interaction/compatibility between deposited $FePO_4$ and α-Fe_2O_3 has a decisive effect on the overall electrocatalytic activity of the resultant electrodes; $FePO_4$ only showed synergetic effect on the overall electrocatalytic activity of α-Fe_2O_{3NR} and α-Fe_2O_{3NS}. The rate constant for the electro-reduction of H_2O_2 on $FePO_4$ modified α-Fe_2O_{3NR} (α-Fe_2O_{3NR}|$FePO_4$) is highest, but $FePO_4$ modified α-Fe_2O_{3NS} (α-Fe_2O_{3NS}|$FePO_4$) showed best overall electrocatalytic activity due to its relatively higher surface area. Furthermore, dissolved oxygen showed negligible interference on the activity of α-Fe_2O_{3NR}|$FePO_4$ and α-Fe_2O_{3NS}|$FePO_4$, which makes them as promising sensing materials in oxidase-based electrochemical sensors.

Introduction

Development of a highly sensitive and reliable hydrogen peroxide (H_2O_2) electrochemical sensor is of great importance not only because H_2O_2 has been identified as a chemical threat to the environment and one of major factors causing the diseases,[1] but also it a frequent intermediate involved in many important oxidase-catalyzed chemical processes, such as glucose oxidation catalysed by glucose oxidase (GOD) (Eqs. 1-2)[2]:

$$\text{glucose} + \text{GOD}-\text{FAD} \rightleftharpoons \text{gluconolactone} + \text{GOD}-\text{FADH}_2 \quad (1)$$

$$O_2 + \text{GOD}-\text{FADH}_2 \longrightarrow H_2O_2 + \text{GOD}-\text{FAD} \quad (2)$$

H_2O_2 is an electroactive species that can be oxidized or reduced electrochemically, and therefore, the electrochemical detection of chemicals involved in oxidase-catalyzed chemical processes can be achieved by detection of H_2O_2. Some oxidase-based electrochemical sensors that utilize the anodic current from the electrooxidation of H_2O_2 as the output signal have been developed, but this kind of sensors often suffer the interferences from some common electro-oxidizable species, such as ascorbic acid and uric acid existing in the biological samples.[3] As a result, to minimize the interference and enhance the selectivity of the oxidase-based electrochemical sensors, the development of oxidase-based electrochemical sensors that use the cathodic current from the electroreduction of H_2O_2 as the output signal is preferential. However, in this case, dissolved oxygen, required to re-oxidize oxidase (e.g., Eq. 2) becomes a potential interfering species as oxygen can also be reduced electrochemically. Therefore, an electrocatalyst that can selectively catalyse the reduction of H_2O_2 against the reduction of O_2 is highly required for constructing oxidase-based electrochemical sensors operated in the cathodic regime.

Many materials have been explored as an active species catalyzing the electrochemical reduction of H_2O_2, including Prussian blue,[4] iron oxides,[5] silver,[6] manganese oxides,[7] copper oxides,[8] *etc*. Among them, iron oxides have been received much attention not only because it is robust, earth abundant, and can be easily synthesized in a cheap way, but also it exhibited peroxidase-like activity.[9] Nevertheless, the mechanism for the electrocatalysis of H_2O_2 by iron oxides is still not well-understood. For example, in previous report,[10] iron oxides nanorods, including β-FeOOH, α-Fe_2O_3, γ-Fe_2O_3, were found to be active for the electrochemical reduction of H_2O_2 in non-phosphate buffer, but only α-Fe_2O_3 was found to be active in the phosphate buffer. The interaction/compatibility between the surface modifier (iron phosphate) and the iron oxide matrix played an important role in determining the overall activity of the iron oxide based material. On the other hand, iron oxides of various nanostructures, such as nanorods,[5f] nanoparticles,[5b-d, 5f, 11] and

No. 1, University Road, National Cheng Kung University, Tainan City 70101, Taiwan. E-mail: cyl44@mail.ncku.edu.tw
Electronic Supplementary Information (ESI) available: Experimental details. See DOI: 10.1039/x0xx00000x

nanotubes,[5e] have been synthesized, and these nanostructured iron oxides have been shown to exhibit enhanced the apparent electrocatalytic activity as compared with the bulk counter-parts. Crystallinity, crystal size, structure, and exposed surface facets, have been shown to have decisive effects on the overall activity of these nanostructured iron oxides.[11c, 12] Nevertheless, most of nanostructured iron oxide were synthesized in powder form, and rarely directly deposit onto the electrode surface, which would not only cause the irreproducibility due to the un-controllable aggregation of these nano-sized iron oxides, but also complicate the following electrode preparation process.

In this work, we report the directly growth of hematite (α-Fe_2O_3) with different nanostructures, including nanorods, nanosheets, and nanoparticles, onto the fluorine-doped tin oxide coated glass substrate (FTO) using chemical bath deposition at mild conditions with follow-up thermal treatment. The effects of nanostructure and the interplay of $FePO_4$ with different nanostructured α-Fe_2O_3 on the overall electrocatalytic properties towards the reduction of H_2O_2 were thoroughly investigated. It was found that synergetic effects of $FePO_4$ with α-Fe_2O_3 greatly enhanced the overall electrocatalytic activity, in terms of overpotential and catalytic current, as compared with $FePO_4$ or α-Fe_2O_3 alone, but this effect occurs only for α-Fe_2O_3 nanorods and nanosheets. In addition, the detection of H_2O_2 by $Fe_2O_{3NR}|FePO_4$ and $Fe_2O_{3NS}|FePO_4$ is insensitive to the dissolved oxygen, which allows their applications to electrochemical detection of key biomolecules involving in oxidase-catalyzed chemical processes.

Experimental section

General consideration. Starting materials for the synthetic part of the work were purchased from commercial suppliers and of the highest available purity for the analytical work. Flourine-doped tin oxide (FTO) coated glass (sheet resistance 7 ohm sq^{-1}, TEC GlassTM 7) substrates (1.0×3.0 cm^2) were cleaned with an ammonia-hydrogen peroxide-deionized water mixture (volume ratio: 1:1:5) at 70 ^oC for 30 min, after which the FTO substrates were dried at room temperature under nitrogen purge. Hydrogen peroxide stock solution (0.5 M) was prepared before each experiment by direct dilution of hydrogen peroxide (H_2O_2, 30wt%) with electrolyte solutions, of different pHs, either containing (i) sodium phosphate (0.1 M) and sodium sulfate (0.1 M), or (ii) sodium sulfate (0.1 M). Deionized water (DIW) was used throughout the work.

Preparation of the FTO|α-Fe_2O_{3NR}, FTO|α-Fe_2O_{3NS}, and FTO|α-Fe_2O_{3NP} electrodes. The FTO|α-Fe_2O_{3NR} electrode was prepared by first growing akagenite nanorods (NR) onto the FTO substrate using chemical bath deposition (CBD) in an aqueous solution containing 1.0 M urea and 0.15 M iron chloride at 90 ^oC for 4 h, followed by thermal conversion of akagenite NRs to α-Fe_2O_{3NR} at 500 ^oC for 1 h. The α-Fe_2O_3 nanosheets (α-Fe_2O_{3NS}) were grown onto the FTO substrate, designated as FTO|α-Fe_2O_{3NS}, by CBD in an aqueous solution containing 0.75 M urea and 0.15 M iron nitrate at 90 ^oC for 4 h and follow-up thermal treatment at 500 ^oC for 1 h. The α-Fe_2O_3 nanoparticles (α-Fe_2O_{3NP}) were grown onto the FTO substrate, designated as FTO|α-Fe_2O_{3NP}, by CBD in an aqueous solution containing 2.0 M urea and 0.15 M iron nitrate at 90 ^oC for 24 h and follow-up thermal treatment at 500 ^oC for 1 h. The exposed area of the FTO substrate for growing nanostructured hematite was kept at 2.0 cm^2.

Physical Characterization. The surface morphology of the electrodes was characterized using a Hitachi SU-8010 scanning electron microscope (SEM). X-ray diffraction (XRD) analyses were carried out using an Ultima IV (Rigaku Co., Japan) X-ray diffractometer. The surface composition of the films was verified by X-ray photoelectron spectroscopy (XPS, PHI 5000 VersaProbe system, ULVAC-PHI, Chigasaki, Japan), using a microfocused (100 µm, 25 W) Al X-ray beam, with a photoelectron take off angle of 45°. The Ar^+ ion source for XPS (FIG-5CE) was controlled by using a floating voltage of 0.2 kV. The binding energies obtained in the XPS analyses were corrected for specimen charging, by referencing the C 1s peak to 285.0 eV.

Electrochemical Characterization. Electrochemical characterizations on the electrocatalytic properties of the nanostructured hematite modified electrodes were performed with a CHI 440 electrochemical workstation (CH Instruments, Inc., USA) at room temperature and all potentials are reported against Ag/AgCl (saturated KCl). A conventional three-electrode electrochemical cell was employed with nanostructure hematite modified electrodes (exposed area of ~1.0 cm^2) as the working electrode, Pt foil (exposed area 4.0 cm^2) as counter electrode, and Ag/AgCl as reference electrode. Prior to experiments, all hematite modified electrodes were pretreated either in (i) phosphate buffer solution (PBS, pH 7) containing sodium phosphate (0.1 M) and sodium sulfate (0.1 M), or in (ii) sodium sulfate (0.1 M, pH 7), using cyclic voltammetry (CV) at a scan rate of 50 mV s^{-1} in the potential window between -0.7 V and +0.4 V (*vs*. Ag/AgCl) until the CV curves became stabilised. The sensitivities of all the hematite modified electrodes determined by CV were the slopes of the curves of cathodic peak current density vs. H_2O_2 concentration. A suitable operating potential in the limiting current plateau region for the amperometric detection of H_2O_2 was determined using linear sweep voltammetry (LSV) at a scan rate of 0.1 mV s^{-1} in PBS (pH 6) containing 0 mM and 4.95 mM H_2O_2. After obtaining the operating potential, which is -0.3 V *vs*. Ag/AgCl, the amperometric detection of H_2O_2 was carried out in PBS (pH 6) under constant magnetic stirring. The current density responses to the changes H_2O_2 concentration were collected, and the calibration curve for detection of H_2O_2 was then constructed. All the electrochemical measurements were repeated at least three times.

Results and discussion

Synthesis of the nanostructured hematite electrodes. All nanostructured hematite (α-Fe_2O_3) were directly grown on to FTO by chemical bath deposition at mild conditions and follow-up thermal treatment at 500 ^oC for 1 h (see ESI for

details). The XRD analyses (Figure S1) shows that all deposited materials were converted into hematite after thermal treatment. As revealed in the SEM images, shown in Figure 1, the nanostructure of α-Fe_2O_3 can be controlled by tuning the composition of the bath solution and the reaction times. For example, nanorods array (α-Fe_2O_{3NR}) can be grown in $FeCl_3$-urea bath solution system, whereas nanosheets (α-Fe_2O_{3NS}) and nanoparticles (α-Fe_2O_{3NP}) can be grown in $Fe(NO_3)_3$-urea bath solution system. The adsorption of anions (Cl^-, CO_3^{2-}, NO_3^-) to specific crystal face and their relative concentrations influence the preferential growth direction of crystal, and therefore, the different nanostructures are created. The detailed growth mechanism will be submitted to elsewhere soon. The relative effective surface area for these nanostructured α-Fe_2O_3 was determined by measuring double-layer capacitance using cyclic voltammetry, [13] and the results (Figure S2) reveal that the relative effective surface area (α-Fe_2O_{3NR}: α-Fe_2O_{3NS}: α-Fe_2O_{3NP}) is 1.00: 1.58: 1.74.

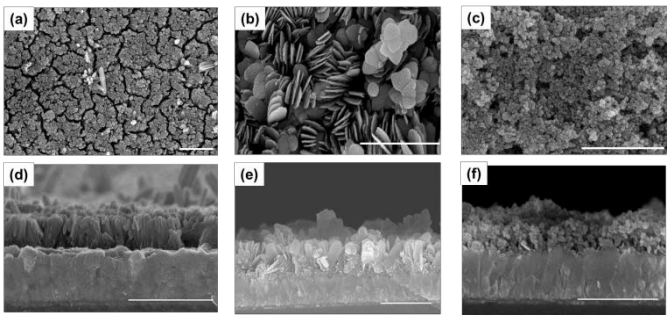

Figure 1 SEM of (a, d) α-Fe_2O_{3NR}, (b, e) α-Fe_2O_{3NS}, (c, f) α-Fe_2O_{3NP}. Scale bar: 1 μm.

Electrochemical characterization. α-Fe_2O_3 is studied in this work as we found that only α-Fe_2O_3 is compatible with *in-situ* deposited iron phosphate ($FePO_4$) in phosphate buffer.[10] As the formation of $FePO_4$ on α-Fe_2O_3 surface during the electrochemical detection of H_2O_2 in phosphate buffer solution (PBS) is inevitable, and to ensure the surface of all the nanostructured α-Fe_2O_3 modified electrodes are fully covered with $FePO_4$, all the nanostructured α-Fe_2O_3 modified electrodes were pre-treated in 0.1 M PBS solution (pH 7) with cyclic voltammetry (CV) from +0.4 to -0.7 V vs. Ag/AgCl at a scan rate of 50 mV s^{-1} until the redox peaks of $FePO_4$ saturated. Figure 2 shows the XPS spectra of Fe 2p, O 1s, and P 2p for all three nanostructured α-Fe_2O_3 electrodes before and after CV pre-treatment. A positive shift (from ~710.9 to 711.3 eV) in binding energy (BE) of the Fe 2p peak after the pre-treatment was noticed for all the electrodes (Figures 2a-c). In addition, the appearance of additional shoulder in O 1s spectra at a BE of 531.5 eV (Figures 2d-f) along with the peak in P 2p spectra at a BE of 133.2 eV (Figures 2g-i) after the pre-treatment were also observed for all the electrodes.

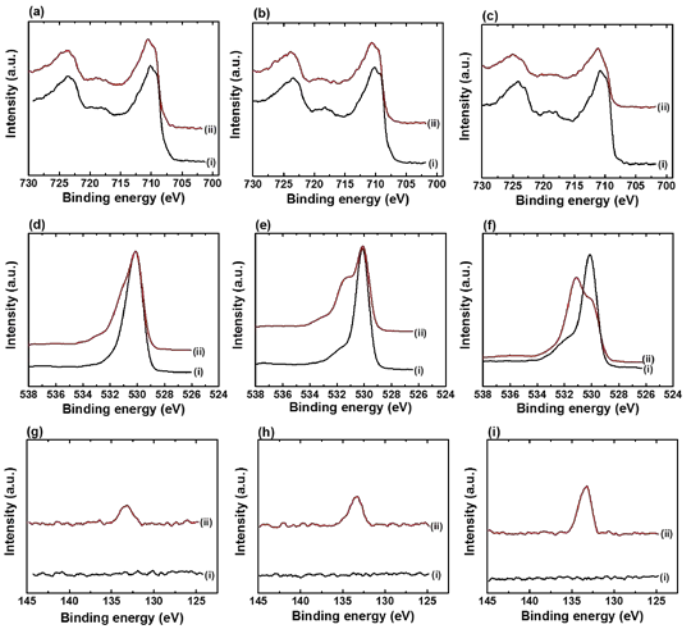

Figure 2 XPS spectra of the pretreated (a, d, g) α-Fe_2O_{3NR}, (b, e, h) α-Fe_2O_{3NS}, and (c f, i) α-Fe_2O_{3NP} (i) before and (ii) after CV-pretreatment. (a-c) Fe 2p region, (d-f) O 1s region, and (g-i) P 2p region

Figure 3 shows the CVs of all the pre-treated nanostructured α-Fe_2O_3 modified electrodes in the PBS (pH 7) at different scan rates (*v*) and the corresponding plots of the peak current density (J_p) vs. *v* are shown in Figure S3. It can be found that the all the pre-treated electrodes exhibited reversible redox peaks which are characteristic to $FePO_4$,[14] and the relationship between J_p with *v* is linear (see Figure S3), which suggests that the deposited species strongly absorbed onto the electrode surface after the pre-treatment. The above observations (Figures 2-3) suggest $FePO_4$ formed during the pre-treatment process. In addition, the slopes of the plot J_{pc} vs *v* for α-Fe_2O_{3NR}|$FePO_4$, α-Fe_2O_{3NS}|$FePO_4$, and α-Fe_2O_{3NP}|$FePO_4$ are found to be -8.38, -18.45, and -2.72, respectively, and the ratio of the relative amount of the deposited $FePO_4$ on the pre-treated α-Fe_2O_{3NR}, α-Fe_2O_{3NS}, and α-Fe_2O_{3NP} can be induced according to Eq. 3, which is 1.00: 2.20: 0.32. Nevertheless, from the XPS analyses, it was found that the elemental ratio of P/Fe for α-Fe_2O_{3NR}|$FePO_4$, α-Fe_2O_{3NS}|$FePO_4$, and α-Fe_2O_{3NP}|$FePO_4$ are 0.26, 0.47, and 0.85, respectively. These findings suggest that the surface of α-Fe_2O_{3NP} prefers the adsorption of phosphate ions over the deposition of $FePO_4$.

$$J_p = \frac{n^2F^2}{4RT}\Gamma_O^* v \qquad (1)$$

Where J_p is peak current density, n is number of electron transfer, F is the Faraday constant, R is gas constant, T is temperature, and Γ_O^* is the amount of absorbed electroactive species. For the clarification, the pre-treated α-Fe_2O_{3NR}, α-Fe_2O_{3NS}, and α-Fe_2O_{3NP} in PBS are designated as α-Fe_2O_{3NR}|$FePO_4$, α-Fe_2O_{3NS}|$FePO_4$, and α-Fe_2O_{3NP}|$FePO_4$, respectively, in the following discussion.

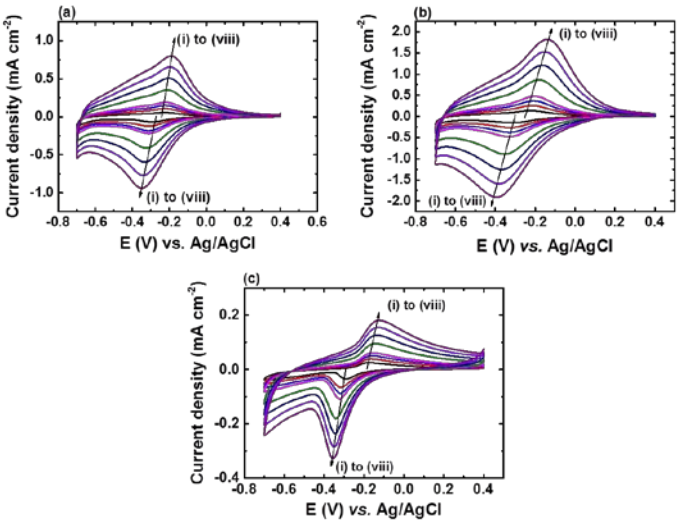

Figure 3 Cyclic voltammetry of the pretreated (a) α-Fe_2O_{3NR}, (b) α-Fe_2O_{3NS}, and (c) α-Fe_2O_{3NP} in 0.1 M PBS (pH 7) at various scan rates. Scan rates for (i), (ii), (iii), (iv), (v), (vi), (vii), and (viii) are 5, 10, 15, 20, 40, 60, 80, and 100 mV s^{-1}, respectively.

Figure 4 shows the CVs of the FTO, α-Fe_2O_{3NR}|$FePO_4$, α-Fe_2O_{3NS}|$FePO_4$, and α-Fe_2O_{3NP}|$FePO_4$ at a scan rate of 20 mVs^{-1} in PBS solution (pH 7) containing H_2O_2 of various concentrations. The cathodic peak current densities (J_{pc}) and corresponding peak potentials (E_{pc}) of all the electrodes in presence of 4.95 mM H_2O_2 are also summarized in Table 1. It can be found that all $FePO_4$ modified α-Fe_2O_3 electrodes exhibited better electrocatalytic activity, in terms of J_{pc} and E_{pc}, than FTO substrate. In addition, J_{pc} at E= -0.30 V *vs*. Ag/AgCl (r_1) increased and J_{pa} at E= -0.22 V *vs*. Ag/AgCl (o_1) decreased upon the addition of H_2O_2 for α-Fe_2O_{3NR}|$FePO_4$, α-Fe_2O_{3NS}|$FePO_4$, and α-Fe_2O_{3NP}|$FePO_4$, which indicates that the electrochemical process at peak r_1 involves electrocatalytic EC' mechanism, and the deposited $FePO_4$ is the active species responsible for the electrochemical process. In addition, an additional cathodic peak (r_2) at E= -0.18 V *vs*. Ag/AgCl appeared upon the addition of H_2O_2 to α-Fe_2O_{3NR}|$FePO_4$ and α-Fe_2O_{3NS}|$FePO_4$, and as this peak is more sensitive to H_2O_2 than peak r_1, peak r_2 outpaced peak r_1 at H_2O_2 concentration of higher than 3.31 mM. Figures 5a-c show the CVs of α-Fe_2O_{3NR}|$FePO_4$, α-Fe_2O_{3NS}|$FePO_4$, and α-Fe_2O_{3NP}|$FePO_4$, respectively, in PBS containing 1.66 mM H_2O_2 at various pHs ranging from 4 to 7. It can be found that the E_{pc} for peak r_1 for all the α-Fe_2O_3 modified electrodes shifted to more negative side as the solution pH was increased, which reflects the redox behavior of $FePO_4$, whereas E_{pc} of peak r_2 (only for α-Fe_2O_{3NR}|$FePO_4$ and α-Fe_2O_{3NS}|$FePO_4$) was insensitive to the change in solution pH. Figure 5d shows the sensitivities, *i.e.*, the slope of the curve of J_{pc} vs. H_2O_2 concentration, of α-Fe_2O_{3NR}|$FePO_4$, α-Fe_2O_{3NS}|$FePO_4$, and α-Fe_2O_{3NP}|$FePO_4$, towards the electrochemical reduction of H_2O_2 at various solution pHs. It can be found that all the electrodes showed best sensitivity at pH 6, and α-Fe_2O_{3NS}|$FePO_4$ exhibited the highest sensitivity among the three kinds of α-Fe_2O_3 modified electrodes. Figure S4 shows the chronoamperometric response of α-Fe_2O_{3NS}|$FePO_4$, at an applied potential of -0.3 V *vs*. Ag/AgCl, after successive addition of the H_2O_2 solution of various concentrations into deaerated 0.1 M PBS (pH 6). It can be found that the current response increased linearly with the increase in H_2O_2 concentration. The sensitivity, *i.e.*, the slope of the calibration curve (shown in the inset of Figure S4) was found to be 225.0 ± 19.9 μA cm^{-2} mM^{-1}. Besides, the sensor response reached 95% of the steady-state value within 10 s upon the addition of H_2O_2. Furthermore, the limit of detection (signal to noise ratio =3) of 3.4 ± 0.5 μM can be achieved.

In previous report,[10] we proposed the EC' mechanisms for peak r_1 (Eqs. 4-5) and peak r_2 (Eqs. 6-7):

$$FePO_{4(s)} + e^- + H^+ \rightleftharpoons Fe^{2+}_{(ad)} + HPO_4^{2-} \quad (2)$$

$$Fe^{2+}_{(ad)} + H_2O_2 + HPO_4^{2-} \rightleftharpoons FePO_4 + H_2O + OH\bullet \quad (3)$$

$$OH\bullet + e^- \rightarrow OH^- \quad (4)$$

$$OH^- + H^+ \rightleftharpoons H_2O \quad (5)$$

The pH-insensitive reduction peak r_2 was found to be related to the intrinsic catalytic property of α-Fe_2O_3 itself, and electron probably comes from the active site, that is, Fe(II) species in the electro-reduced α-Fe_2O_3 under cathodic conditions.[15] The lack of this peak for the case of α-Fe_2O_{3NP}|$FePO_4$ implies that this intrinsic catalytic property is structure-dependent or repressed by other factors, such as the electrolyte or the deposited $FePO_4$. It is worth noting that although α-Fe_2O_{3NP}|$FePO_4$ has the highest surface area (Figure S2), without synergetic with this activity, it showed least overall activity, in terms of I_{pc} and E_{pc}, among the three α-Fe_2O_{3NP} modified electrodes. The higher overpotential required for α-Fe_2O_{3NP}|$FePO_4$ to reduce H_2O_2 is in agreement with previous reports.[5c, 5d, 12a]

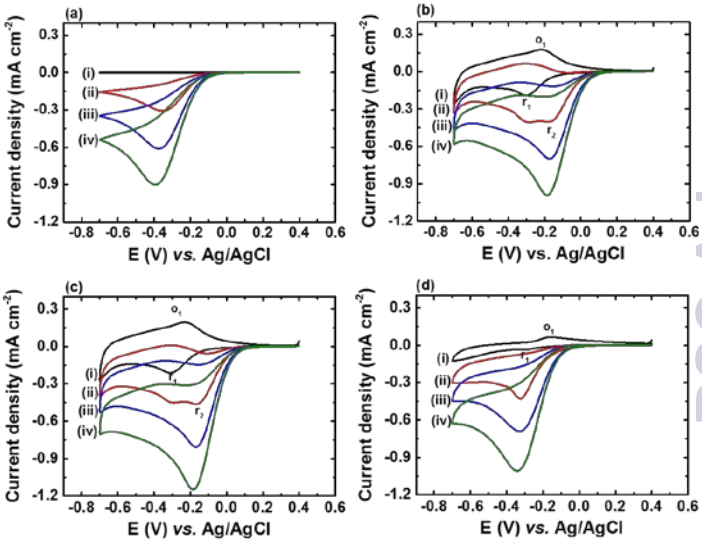

Figure 4 Cyclic voltammetry, recorded at a scan rate of 20 mV s^{-1}, of (a) FTO, (b) α-Fe_2O_{3NR}|$FePO_4$, (c) α-Fe_2O_{3NS}|$FePO_4$, and (d) α-Fe_2O_{3NP}|$FePO_4$ in 0.1 M PBS solution (pH 7) containing H_2O_2 of various concentrations. Concentration of H_2O_2 used for curve (i), (ii), (iii), and (iv) are 0, 1.66, 3.31, and 4.95 mM, respectively.

Table 1 Summary of values of J_{pc} and E_{pc} of the FTO and nanostructured $FePO_4$ modified α-Fe_2O_3 electrodes.

	Sample			
	FTO	α-Fe_2O_{3NR}|$FePO_4$	α-Fe_2O_{3NS}|$FePO_4$	α-Fe_2O_{3NP}|$FePO_4$
J_{pc}[a] (mA cm^{-2})	-0.996 ± 0.099	-1.025 ± 0.035	-1.236 ± 0.074	-1.008 ± 0.035
E_{pc}[b] (V vs. Ag/AgCl)	-0.373 ± 0.026	-0.190 ± 0.003	-0.179 ± 0.003	-0.345 ± 0.005

[a]: cathodic peak current density; [b]: cathodic peak potential. All parameters are determined in 0.1 M PBS solution (pH 7) containing 4.95 mM H_2O_2.

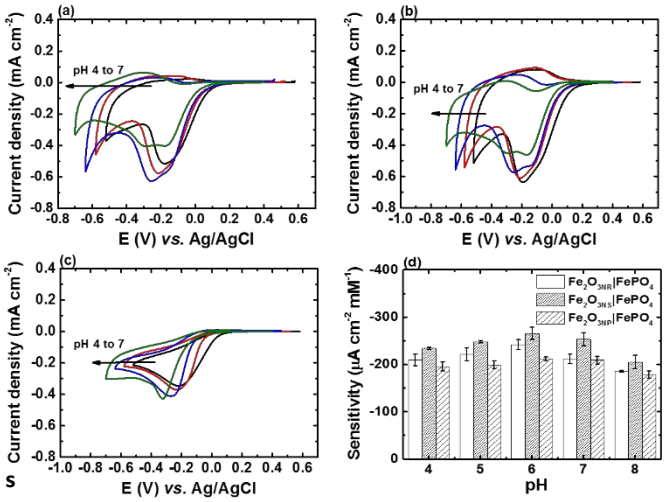

Figure 5 (a)-(c) Cyclic voltammetry, recorded at a scan rate of 20 mV s^{-1}, of α-Fe_2O_{3NR}|$FePO_4$ (a), α-Fe_2O_{3NS}|$FePO_4$ (b), and α-Fe_2O_{3NP}|$FePO_4$ (c) in 0.1 M PBS containing 1.66 mM H_2O_2 at various pHs ranging from 4 to 7. (d) The sensitivities of α-Fe_2O_{3NR}|$FePO_4$, Fe_2O_{3NS}|$FePO_4$, and Fe_2O_{3NP}|$FePO_4$ in 0.1 M PBS of various pHs.

Figures 6a-c shows the chronoamperograms for all the α-Fe_2O_3 modified electrodes at an applied potential of -0.3 V vs. Ag/AgCl in 0.1 M PBS solution containing H_2O_2 of various concentrations. It can be found that all the nanostructured $FePO_4$ modified α-Fe_2O_3 modified electrodes exhibited catalytic current densities that are linearly proportional to the H_2O_2 concentration. The rate constants of the reduction of H_2O_2 on the nanostructured $FePO_4$ modified α-Fe_2O_3 modified electrodes can be derived from Figures 6a-c and the Eqs. 6-7:[16]

$$\frac{J_{cat}}{J_L} = \lambda^{0.5}\left[\pi^{0.5}\mathrm{erf}(\lambda^{0.5}) + \frac{\exp(-\lambda)}{\lambda^{0.5}}\right] \qquad (6)$$

where J_{cat} is the catalytic current density in presence of H_2O_2, J_L is the current density in the absence of H_2O_2, and $\lambda = k_sC^*t$, where k_s, C*, and t are the apparent rate constant, bulk H_2O_2 concentration, and the elapsed time, respectively. When the value of λ is larger than 1.5, the value of erf ($\lambda^{0.5}$) approaches to 1, and exp(-λ) term can be ignored, and as a result, Eq. (6) can be simplified to Eq. (7):

$$\frac{J_{cat}}{J_L} = \pi^{0.5}\lambda^{0.5} \qquad (7)$$

The values of k_s for the reduction of H_2O_2 on α-Fe_2O_{3NR}|$FePO_4$, α-Fe_2O_{3NS}|$FePO_4$, and α-Fe_2O_{3NP}|$FePO_4$, determined from the slopes of plots of J_{cat}/J_L versus $t^{0.5}$ in Figure 6d, are found to be 18253.9, 15242.7, and 2037.9 L mol^{-1} s^{-1}, respectively, which further indicates that the kinetics of H_2O_2 reduction process can be further facilitated with the active Fe (II) species in α-Fe_2O_3. Note that although the value of k_s for Fe_2O_{3NR}|$FePO_4$ is higher than that for α-Fe_2O_{3NS}|$FePO_4$, α-Fe_2O_{3NS}|$FePO_4$ exhibited higher overall electrocatalytic activity over Fe_2O_{3NR}|$FePO_4$ as α-Fe_2O_{3NS}|$FePO_4$ has higher surface area.

Figure S5 shows CVs of the FTO, α-Fe_2O_{3NR}, α-Fe_2O_{3NS}, and α-Fe_2O_{3NP} at a scan rate of 20 mV s^{-1} in 0.1 M Na_2SO_4 solution (pH 7) containing H_2O_2 of various concentrations. Note that the deposition of $FePO_4$ is impossible in this electrolyte, and the observed activity from all the α-Fe_2O_3 reflects their intrinsic activity. Values of I_{pc} and E_{pc} of all the electrodes in presence of 4.95 mM H_2O_2 are also summarized in Table S1. As revealed, α-Fe_2O_{3NP} showed the highest apparent electrocatalytic activity, in terms of I_{pc} and E_{pc}, among the four electrodes, which could be attributed to its highest surface area. In addition, as shown in Figure S6, all the three nanostructured α-Fe_2O_3 modified electrodes exhibited a pH-independent current response to H_2O_2, which suggests the reaction catalysed by these nanostructured α-Fe_2O_3 should be the same, and therefore, the repressed activity of α-Fe_2O_{3NP}|$FePO_4$ in phosphate buffer could be attributed to the unfavourable interaction between α-Fe_2O_{3NP} and deposited $FePO_4$ and/or phosphate ions. It has been reported that the adsorbed phosphate ions would inhibit the reduction of α-Fe_2O_3,[17] which in turn inhibit the formation of Fe(II) species responsible for the reduction of H_2O_2.

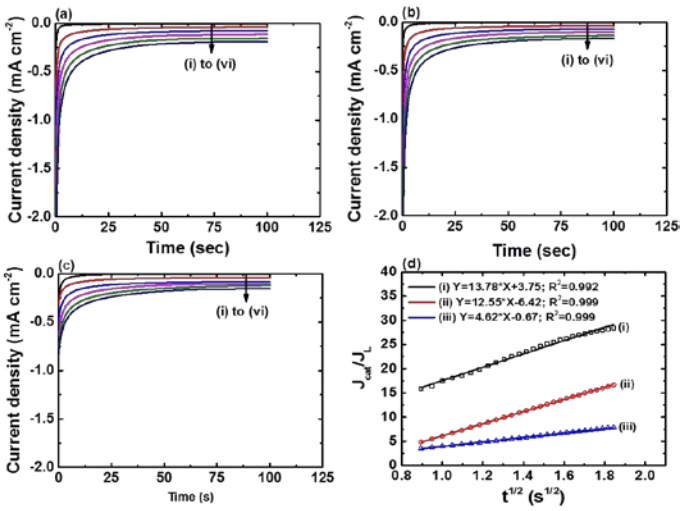

Figure 6 (a)-(c) Chronoamperograms of α-Fe_2O_{3NR}|$FePO_4$ (a), α-Fe_2O_{3NS}|$FePO_4$ (b), and α-Fe_2O_{3NP}|$FePO_4$ (c) recorded at an applied potential of -0.3 V *vs.* Ag/AgCl in 0.1 M PBS (pH 6) containing H_2O_2 of various concentrations. H_2O_2 concentrations used for curves (i), (ii), (iii), (iv), (v), and (vi) are 0, 0.66, 1.32, 1.98, 2.64, and 3.30 mM, respectively. (d) Plots of J_{cat}/J_L vs. $t^{1/2}$ for (i) α-Fe_2O_{3NR}|$FePO_4$, (ii) α-Fe_2O_{3NS}|$FePO_4$, and (iii) and α-Fe_2O_{3NP}|$FePO_4$ using the curves obtained with 0 mM H_2O_2 and 3.30 mM H_2O_2 in (a)-(c).

Figure 7 shows the CVs of α-Fe_2O_{3NR}|$FePO_4$, α-Fe_2O_{3NS}|$FePO_4$, and α-Fe_2O_{3NP}|$FePO_4$ in 0.1 M PBS (pH 6) containing various H_2O_2 concentration under N_2 and air atmospheres. The sensitivities of α-Fe_2O_{3NR}|$FePO_4$, α-Fe_2O_{3NS}|$FePO_4$, and α-Fe_2O_{3NP}|$FePO_4$ obtained from the data in Figure 7 are shown in Figure S7. When comparing the CV responses in absence of H_2O_2 under different atmospheres, it can be found that I_{pc} of peak r_1 increased and I_{pa} of peak o_1 decreased for all the $FePO_4$ modified α-Fe_2O_3 electrodes, which indicates that the deposited $FePO_4$ is active in catalysing the electrochemical reduction of dissolved oxygen in PBS. In addition, the peak r_2 appeared only after the addition of H_2O_2 regardless of background atmosphere, which suggests that the Fe(II) sites in electro-reduced α-Fe_2O_3 is active for the reduction of H_2O_2 but not for the reduction of dissolved oxygen. As a result, the dissolved oxygen showed little effect on the sensitivity of α-Fe_2O_{3NR}|$FePO_4$ and α-Fe_2O_{3NS}|$FePO_4$ towards the electrochemical reduction of H_2O_2; the sensitivities of α-Fe_2O_{3NR}|$FePO_4$ and α-Fe_2O_{3NS}|$FePO_4$ towards the electrochemical reduction of H_2O_2 under air atmosphere remained 96.5 ± 4.3% and 94.7 ± 4.7%, respectively, of those under N_2 atmosphere. In contrast, the sensitivity of α-Fe_2O_{3NP}|$FePO_4$ towards the electrochemical reduction of H_2O_2 under air atmosphere only remained 41.4 ± 3.9% of that at N_2 atmosphere. The significant influence of dissolved oxygen on α-Fe_2O_{3NP}|$FePO_4$ can be attributed to the facts that α-Fe_2O_{3NP}|$FePO_4$ lacks of the Fe(II) sites and the interaction of $FePO_4$ with dissolved oxygen suppresses the reaction between $FePO_4$ and H_2O_2. The low interference from oxygen for α-Fe_2O_{3NR}|$FePO_4$ and α-Fe_2O_{3NS}|$FePO_4$ makes them as a potential candidate material for the detection of biomolecules involving in oxidase-catalysed chemical processes.

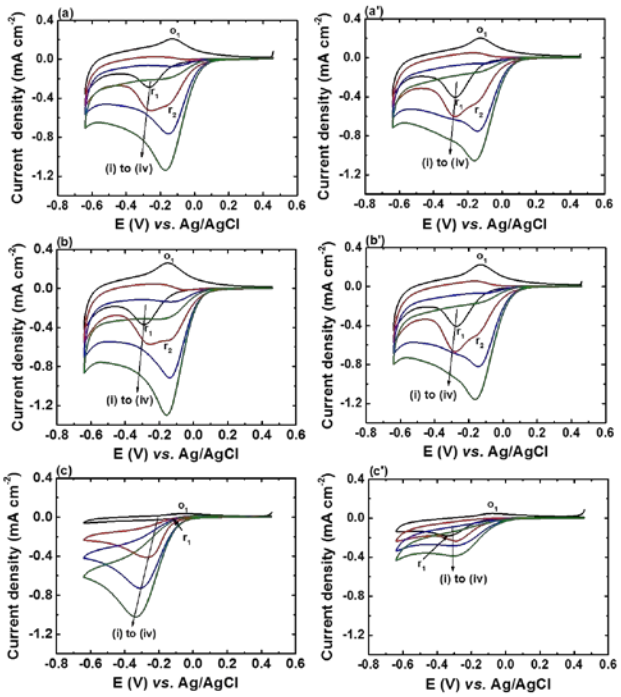

Figure 7 Cyclic voltammetry, recorded at a scan rate of 20 mV s^{-1}, of (a, a') α-Fe_2O_{3NR}|$FePO_4$, (b, b') Fe_2O_{3NS}|$FePO_4$, (c, c') Fe_2O_{3NP}|$FePO_4$ in 0.1 M PBS (pH 6) containing various H_2O_2 concentrations under (a-c) N_2, and (a'-c') air atmospheres. H_2O_2 concentrations used for curves (i), (ii), (iii), and (iv) are 0, 1.66, 3.31, and 4.95 mM, respectively.

Conclusions

α-Fe_2O_3 nanorods, nanosheets, and nanoparticles were successfully synthesized using chemical bath deposition and their electrocatalytic properties were thoroughly examined in phosphate buffer and non-phosphate electrolyte. In phosphate buffer, the *in-situ* deposited $FePO_4$ exhibited synergetic effect on the activity of α-Fe_2O_3 nanorods and nanosheets only, and the surface modification of $FePO_4$ on these two nanostructured α-Fe_2O_3 greatly enhanced their overall electrocatalytic activity as compared with $FePO_4$ or α-Fe_2O_3 alone. The active sites, Fe(II), in α-Fe_2O_3 nanorods and nanosheets are insensitive to the dissolved oxygen, and makes them as the potential electrode material for the fabrication of selective and sensitive H_2O_2 or related electrochemical sensors.

Acknowledgements

This research was, in part, supported by the Ministry of Education, Taiwan, R.O.C. The Aim for the Top University Project to the National Cheng Kung University (NCKU). Financial support from the Ministry of Science and Technology of Taiwan (MOST 104-2221-E-006 -235- and 104-ET-E-006-004-ET) are also gratefully acknowledged.

Notes and references

‡ Footnotes relating to the main text should appear here. These might include comments relevant to but not central to the matter under discussion, limited experimental and spectral data, and crystallographic data.

1 E. Nossol and A. J. Gorgatti Zarbin, *J. Mater. Chem.*, 2012, **22**, 1824-1833.
2 J. Wang, *Chem. Rev.*, 2008, **108**, 814-825.
3 (a) J. Hrbac and R. Kohen, *Drug Develop. Res.*, 2000, **50**, 516-527; (b) R. Kohen, E. Vellaichamy, J. Hrbac, I. Gati and O. Tirosh, *Free Radic. Biol. Med.*, 2000, **28**, 871-879.
4 (a) A. A. Karyakin and E. E. Karyakina, *Sen. Actuators B-Chem.*, 1999, **57**, 268-273; (b) A. A. Karyakin, E. A. Puganova, I. A. Budashov, I. N. Kurochkin, E. E. Karyakina, V. A. Levchenko, V. N. Matveyenko and S. D. Varfolomeyev, *Anal. Chem.*, 2004, **76**, 474-478.
5 (a) Z. L. Liu, B. Zhao, Y. Shi, C. L. Guo, H. B. Yang and Z. A. Li, *Talanta*, 2010, **81**, 1650-1654; (b) L. Zhang, Y. Zhai, N. Gao, D. Wen and S. Dong, *Electrochem. Commun.*, 2008, **10**, 1524-1526; (c) J. Hrbac, V. Halouzka, R. Zboril, K. Papadopoulos and T. Triantis, *Electroanal.*, 2007, **19**, 1850-1854; (d) L. Zhang, Y. H. Ni, X. H. Wang and G. C. Zhao, *Talanta*, 2010, **82**, 196-201; (e) J. Gong, L. Wang, K. Zhao and D. Song, *Electrochem. Commun.*, 2008, **10**, 123-126; (f) J. Z. Marinho, R. H. O. Montes, A. P. de Moura, E. Longo, J. A. Varela, R. A. A. Munoz and R. C. Lima, *Mater. Res. Bull.*, 2014, **49**, 572-576.

6 (a) C.-Y. Lin, Y.-H. Lai, A. Balamurugan, R. Vittal, C.-W. Lin and K.-C. Ho, *Talanta*, 2010, **82**, 340-347; (b) S. Wu, H. Zhao, H. Ju, C. Shi and J. Zhao, *Electrochem. Commun.*, 2006, **8**, 1197-1203.

7 (a) K. Schachl, H. Alemu, K. Kalcher, J. Jezkova, I. Svancara and K. Vytras, *Anal. Lett.*, 1997, **30**, 2655-2673; (b) J.-H. Lee and H.-G. Hong, *J. Appl. Electrochem.*, 2015, **45**, 1153-1162.

8 (a) X.-M. Miao, R. Yuan, Y.-Q. Chai, Y.-T. Shi and Y.-Y. Yuan, *J. Electroanal. Chem.*, 2008, **612**, 157-163; (b) J. M. Zen, H. H. Chung and A. S. Kumar, *Analyst*, 2000, **125**, 1633-1637.

9 L. Gao, J. Zhuang, L. Nie, J. Zhang, Y. Zhang, N. Gu, T. Wang, J. Feng, D. Yang, S. Perrett and X. Yan, *Nature Nanotechnol.*, 2007, **2**, 577-583.

10 C.-Y. Lin and C.-T. Chang, *Sens. Actuators B-Chem.*, 2015, **220**, 695-704.

11 (a) M. Magro, D. Baratella, G. Salviulo, K. Polakova, G. Zoppellaro, J. Tucek, J. Kaslik, R. Zboril and F. Vianello, *Biosens. Bioelectron.*, 2014, **52**, 159-165; (b) M. Magro, D. Baratella, N. Pianca, A. Toninello, S. Grancara, R. Zboril and F. Vianello, *Sens. Actuators B-Chem.*, 2013, **176**, 315-322; (c) D. Baratella, M. Magro, G. Sinigaglia, R. Zboril, G. Salviulo and F. Vianello, *Biosens. Bioelectron.*, 2013, **45**, 13-18; (d) A. K. Dutta, S. K. Maji, D. N. Srivastava, A. Mondal, P. Biswas, P. Paul and B. Adhikary, *J. Mol. Catal. A-Chem.*, 2012, **360**, 71-77.

12 (a) J. M. Gong, L. Y. Wang, K. Zhao and D. D. Song, *Electrochem. Commun.*, 2008, **10**, 123-126; (b) S. Nath, C. Kaittanis, V. Ramachandran, N. S. Dalal and J. M. Perez, *Chem. Mater.*, 2009, **21**, 1761-1767; (c) S. H. Liu, F. Lu, R. M. Xing and J. J. Zhu, *Chem. Eur. J.*, 2011, **17**, 620-625; (d) N. Puvvada, P. K. Panigrahi, D. Mandal and A. Pathak, *RSC Adv.*, 2012, **2**, 3270-3273.

13 S. Trasatti and O. A. Petrii, *Pure Appl. Chem.*, 1991, **63**, 711-734.

14 (a) F. Marken, D. Patel, C. E. Madden, R. C. Millward and S. Fletcher, *New J. Chem.*, 2002, **26**, 259-263; (b) K. J. McKenzie and F. Marken, *Pure Appl. Chem.*, 2001, **73**, 1885-1894.

15 M. S. Lin and H. J. Len, *Electroanal.*, 2005, **17**, 2068-2073.

16 F. Pariente, E. Lorenzo, F. Tobalina and H. D. Abruna, *Anal. Chem.*, 1995, **67**, 3936-3944.

17 C. Liu, J. M. Zachara, N. S. Foster and J. Strickland, *Environ. Sci. Technol.*, 2007, **41**, 7730-7735.

Table of Content

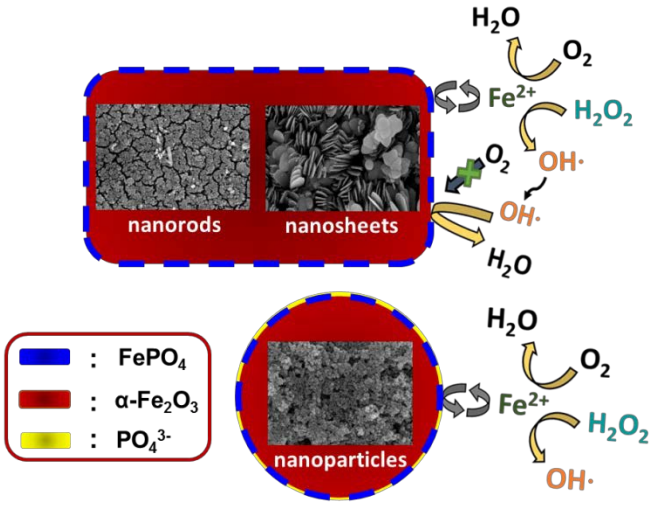

Structure-dependent selectivity of *α*-Fe_2O_3|$FePO_4$ based electrochemical H_2O_2 sensor against dissolved O_2.